Artero-Guerrero, J., Pernas-Sánchez, J., & Teixeira-Dias, F. (2017). Blast wave dynamics: The influence of the shape of the explosive. Journal of Hazardous Materials, 331, 189-199.

doi:https://doi.org/10.1016/j.jhazmat.2017.02.035

Blast wave dynamics: the influence of the shape of the explosive

J. Artero-Guerrero[a], J. Pernas-Sánchez[a], F. Teixeira-Dias[b,*]

[a]*Department of Continuum Mechanics and Structural Analysis, University Carlos III of Madrid, 28911 Leganés, Madrid, Spain*
[b]*School of Engineering, The University of Edinburgh, Edinburgh EH9 3JL, UK*

Abstract

A numerical model is developed to analyse the influence of the shape of a high-explosive on the dynamics of the generated pressure wave. A Multi-Material Arbitrary Lagrangian Eulerian (MM-ALE) technique is used as the CONWEP approach is not adequate to model such situations. Validation and verification of the proposed numerical model is achieved based on experimental data obtained from the bibliography. The numerical model provides relevant information that cannot be obtained from the experimental results. The influence of the mass and shape of the high-explosive is studied and correlated to the dynamics of the generated blast wave through the analysis of peak pressures, time of arrival and impulse. Tests are done with constant mass hemispherical, cylindrical and flat-shaped Formex F4HV samples. A detailed analysis of the generated blast wave is done, along with a thorough comparison between incident and reflected waves. It is concluded that the dynamic effects of the reflected pressure pulses should always be considered in structural design, most relevantly when analysing closed structures where the number of reflections can be significant. The model is proved reliable, concluding that the frontal area of the high-explosive is a determinant driving parameter for the impulse generated by the blast.

Keywords: Blast wave, Multi-Material Arbitrary Lagrangian Eulerian, Fluid Structure Interaction, Impulse, High-explosive

1. Introduction

Anticipating the effects of an explosion is a major task when designing blast protection structures, both for defence or accident mitigation, or in accident/attack reconstruction. From this perspective, the most relevant physical parameters are directly related to the generated pressure pulse (overpressure, time of arrival, etc.), the induced impulse on the structure and the configuration of the blast wave. This paper focuses on this latter aspect and the novel contribution proposed by the authors is the assessment of which geometrical factors — initial shape of the high-explosive (HE) —

*Corresponding author: F. Teixeira-Dias

are most relevant and determinant for the shape of the blast wave, and how this will affect the generated pressure and impulse.

In the past, authors have studied the evolution of the shape of a blast wave when it interacts with structures. Benselama et al. [1] studied the interaction of a blast wave and quadrangular cross-section tunnel structures. These authors performed a set of parametric analyses looking into the effect of the aspect ratio of the cross section of the tunnel and the relative initial position of the explosive on the development of the blast wave. They concluded that geometrical aspects, namely the ratio of the HE mass to the hydraulic diameter of the tunnel, are highly relevant parameters. However, all observations and analyses were based on the assumption that the initial blast wave (i.e. before it interacts with the structure) is spherical.

Other studies, such as the ones by Larcher et al. [2] and Clutter and Stahl [3], adopt a larger scale approach, and discuss the effect of a HE generated blast wave on complex structures such as train carriages and large offshore structures or clusters of structures, but again assuming that the initial shape of the blast wave is spherical. Larcher et al. [2] developed a complex numerical model to analyse the effects of venting on the evolution of pressure and impulse after a detonation. They thoroughly analysed the effect of different venting areas and mass of explosive, both on simple tunnel-like structures and realistic train carriages, effectively contributing to the knowledge that venting areas have a drastic influence on the effects (including injury levels) of an explosion. The earlier study by Clutter and Stahl [3] analyses the interaction of a blast wave generated by a HE detonation on different scenarios with highly complex configurations and geometries, such as industrial sites, urban environments and off-shore facilities. They proposed a novel approach to represent the explosive source term, using an enthalpy formulation, validate this using several shock-tube experiments and further expand their model to study the relevance of the geometrical detailing when modelling complex environment and blast waves.

Most of the publications on this topic, however, are mostly concerned with the interaction effects and the geometry and configuration of surrounding structures, not specifically with the shape of the blast wave front, almost always assuming an initially spherical blast wave, as can be additionally substantiated by the work of Vanderstraeten et al. [4]. Conversely, in the present work the authors are mostly concerned with the relation between the pre-detonation shape of the high-explosive and the post-detonation configuration and shape of the blast wave and the generated pressure and impulse. A numerical model is developed to analyze this and is validated using the experimental results obtained by Lefrancois et al. [5] and Mespoulet et al. [6]. The influence of the mass and shape of the high-explosive is analysed and correlated to the dynamics of the generated blast wave through the analysis of peak pressures, time of arrival and impulse.

2. Numerical modelling

A numerical model is developed to study the influence of the pre-detonation shape of the high-explosive on the blast wave formation and dynamics. For validation purposes, the obtained results are compared to experimental observations by Lefrancois et al. [5] and Mespoulet et al. [6]. These authors used a 14.2 g hemispherical (13.5 [mm] of radius) and a 15 g flat explosive ($120\times60\times1.5$ [mm^3]) to study the influence of different HE shapes on the profile of the blast wave. The composition of the HE used is PETN/rubber with a 89/11 ratio, commercially known as Formex F4HV. The following sections describe in detail the setup of the numerical model was setup in these sections.

2.1. Geometry, domain, boundary conditions and discretisation

The diagram in Figure 1 is an overview of the whole experimental and numerical setup. As can be seen, the high-explosive is positioned at the centre of a 2000×2000 [mm^2] high density concrete wall, designated by incident wall (IW). Four pressure transducers (PI_i with $i = 1, \ldots, 4$) are located along this wall spaced as indicated. A second parallel concrete wall is positioned 570 mm from the incident wall, with two additional pressure transducers (PR_1 and PR_2), designated by reflected wall (RW). The pressure transducers used in the experimental setup were PCB piezoelectric gauges and the explosions were recorded at 30,000 fps using a Photron high speed video camera.

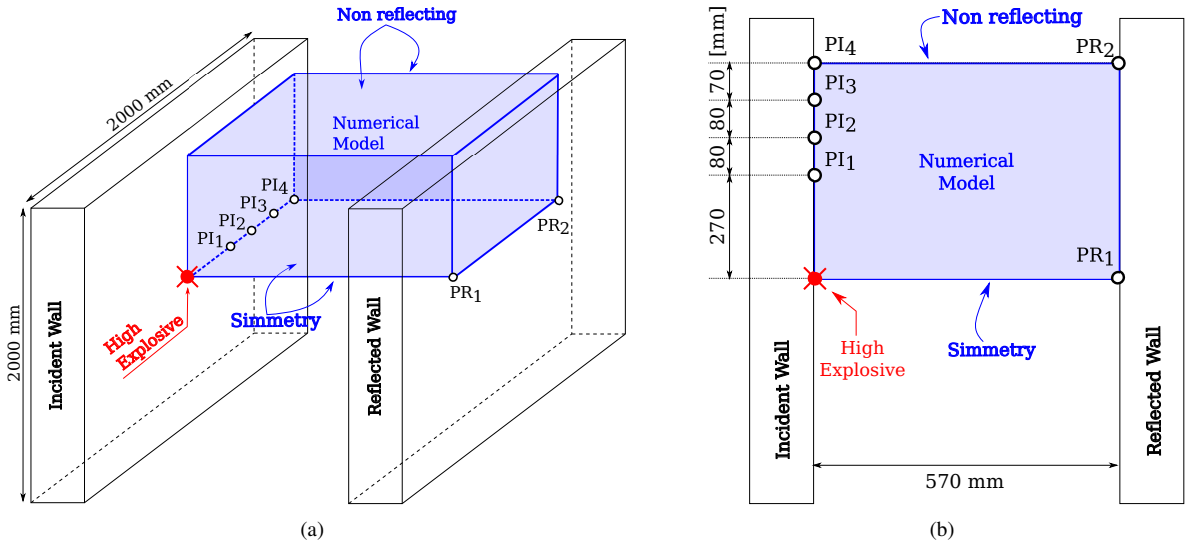

Figure 1: (a) 3D and (b) top views of the experimental setup according to Lefrancois et al. [5]. Highlighted in blue is the physical region that is numerically modelled in the present paper (not to scale).

The commercial finite element analysis (FEA) package LS-Dyna [7] is used to reproduce the experimental tests and ultimately better understand how the initial (pre-detonation) shape of the high-explosive influences the development and propagation of the resulting blast wave. The CONWEP approach is often used to model blast waves and is

implemented in LS-Dyna [8, 9, 10, 11, 12, 13, 14, 15, 16]. However, this method cannot be used in the scope of the work here presented as it is only suited for spherical HE, which will ultimately generate spherical blast wave fronts, regardless of the shape of the HE.

Additionally, adopting a finite element (FE) Lagrangian technique is also not adequate as this approach will fail to accurately reproduce the generation and propagation of the blast wave. This is mostly due to the high levels of deformation and strain that will develop, leading to severe element distortions and ultimately numerical instabilities (e.g. time integration instabilities) [17, 18]. Consequently, the approach adopted to model the generation and propagation of non-spherical blast waves is the Multi-Material Arbitrary Lagrangian Eulerian (MM-ALE) technique. As the numerical mesh is not coupled to material deformation this method is believed to be more efficient in avoiding severe element distortions [19, 20] and, consequently, better handle high velocity fluid-structure interactions (FSI) [21, 22, 23, 24].

In the present work, a fully Eulerian description is used because mesh velocity is set to zero as materials flow through the mesh. However, as the Eulerian description can be considered to be a special case of MM-ALE, the authors still use the MM-ALE designation. The main drawback of this approach is the significant increase in computational cost due to the inclusion of convective terms in the formulation. Therefore, in order to optimise the computational cost, the symmetries of the domain — two symmetry planes — are explored, leading to the numerical domain highlighted in blue in Figure 1, with 570×1140 [mm^2]. The discretisation of the numerical domain relies on a finite element mesh with increasing refinement closer to the location of the high-explosive. By doing this it becomes possible to reproduce the pre-detonation shapes of the explosive accurately. Finite element sizes increase from $2.5 \times 2.5 \times 0.5$ [mm^3] in the region where the HE is positioned to $15 \times 15 \times 5$ [mm^3] away from the detonation point, as can be seen in the generic mesh shown in Figure 3. The element size is chosen following a mesh sensitivity and convergence study, where the accuracy of results regarding the blast wave and computational cost is weighted. All the optimised finite element meshes have around 1.65 million elements, corresponding to approximately 5.1 million degrees-of-freedom. The finite element used is the 8-node solid multi-material element with reduced integration and hourglass control. In this research study the influence of the pre-detonation shape of the HE in the resulting blast wave has been done, to this end the authors adopted the five shapes shown in Figure 2 (dimensions listed in Table 1). The aspect ratio is calculated as the ratio $V/(\pi r^2)$, where V is the volume and r the radius; in the case of the flat geometry the aspect ratio is obtained by $V/(L \cdot w)$, where V is the volume, L the length and w the width.

(a) Hemispherical (b) Cylindrical A (c) Cylindrical B (d) Cylindrical C (e) Flat

Figure 2: Generic shapes of the high-explosives used in the numerical models: (a) hemispherical, (b-d) cylindrical and (e) flat.

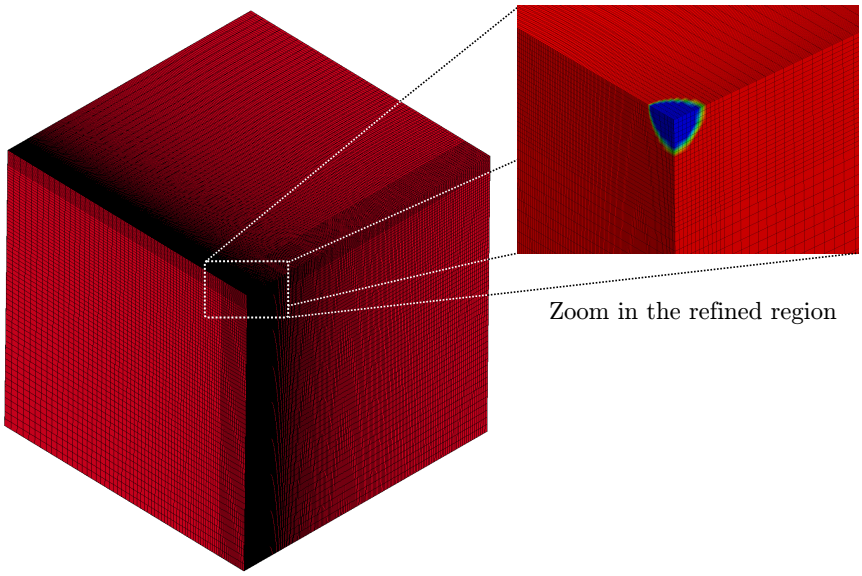

Figure 3: Generic finite element mesh, showing how mesh density changes from the position of the high-explosive to the outer limits of the numerical model domain. Note that only 1/2 of the Semi-spherical high explosive is simulated due to the symmetries.

Table 1: Dimensions and aspect ratios of the different shapes of the high-explosive used in the numerical models.

Model	**Figure**	**Height [mm]**	**Diameter [mm]**	**Aspect ratio**
Hemispherical	2(a)	–	16.8	11.2
Cylindrical A	2(b)	12	16.9	12.0
Cylindrical B	2(c)	8	20.7	8.0
Cylindrical C	2(d)	4	29.3	4.0
Flat	2(e)	1.5	120 (length) × 60 (width)	1.5

Both the incident and the reflected walls are considered as rigid and have consequently been modelled as boundary conditions with restricted normal displacements. In addition to the walls and symmetry planes the outer limits of the numerical domain are defined as non-reflecting boundaries, as indicated in Figure 1.

2.2. Material behaviour

The only materials that need to be defined in the numerical models are the high-explosive (Formex F4HV) and the surrounding air. The behaviour of Formex F4HV is described as a high-explosive material using a Jones-Wilkins-Lee (JWL) equation of state (EOS). The release of chemical energy from the detonation is accounted for in this EOS both from the resulting compression and the programmed detonation [7, 25]. The former defines the detonation when the compression in the material reaches the Chapmant-Jouget pressure P_{CJ} whilst the latter defines the initial detonation time as a function of the detonation velocity D and the location of the detonation point [16]. The JWL model defines the pressure as

$$p = A\left(1 - \frac{\omega}{R_1 v}\right)e^{-R_1 v} + B\left(1 - \frac{\omega}{R_2 v}\right)e^{-R_2 v} + \frac{\omega E}{v} \tag{1}$$

where A, B, R_1, R_2 and ω are material constants, $\nu = \rho_0/\rho$ is the ratio of the initial to the current densities (i.e. the relative volume) and E is the internal specific energy (i.e. per unit volume). Due to the compaction and shaping processes, the real density of the HE and its detonation velocity are not equal for all geometrical configurations. These parameters (density and detonation velocity) are taken from the specifications provided by the manufacturer of the HE [26]. Lefrancois et al. [5] observed very similar pressure pulses when comparing the detonation of a hemispherical Formex F4HV and TNT. Moreover, TNT has a $1:1$ weight equivalence with Formex for pressure effect, so all the remaining properties are assumed identical to TNT parameters obtained from Dobratz et al. [5, 25] listed in Table 2.

Air is assumed to behave as an ideal gas, leading to an equation of state that can be defined as

$$p = (\gamma - 1)\,\frac{\rho}{\rho_0} E \tag{2}$$

where γ is the ratio of specific heats ($\gamma = c_\mathrm{p}/c_\mathrm{v}$). The material properties of the air are also listed in Table 2 and were obtained from Tabatabaei et al. [27].

Table 2: Material properties for the high-explosive (Formex F4HV) and air used in the MM-ALE numerical models.

Property	**Units**	**Formex F4HV**	**Air**
ρ_0	kg/m^3	1390	1.23
E	GJ/m^3	7.0	2.58×10^{-4}
D	m/s	6500	–
P_CJ	GPa	21.0	–
A	GPa	371.0	–
B	GPa	3.23	–
R_1	–	4.15	–
R_2	–	0.95	–
ω	–	0.3	–
γ	–	–	1.4

3. Numerical Results

3.1. Validation of the numerical model

Before proceeding to the analysis of the effect of the pre-detonation HE shape on the blast wave dynamics it is necessary to validate the proposed numerical model. In order to do this, the pressures at the pressure transducers PI_i ($i = 1, \ldots 4$) and PR_j ($j = 1, 2$) were obtained from the experimental tests and are compared to the corresponding numerical values. The relative impulse, obtained by integrating the pressure pulses, is then used as the validation parameter since it represents the impulse transmitted to a structure due to the blast wave.

The experimental and numerical pressure-time histories from the detonation of an hemispherical mass of 14.2 g of Formex F4HV are shown in Figure 4. The difference between the pressure pulses measured in the incident and

the reflected walls by transducers PI_i and PR_j, respectively, is immediately evident from these results. The negative overpressure phase of the blast wave is well captured by the numerical model although this is not clearly visible in the experimental results, most probably due to the short duration of the pressure signal.

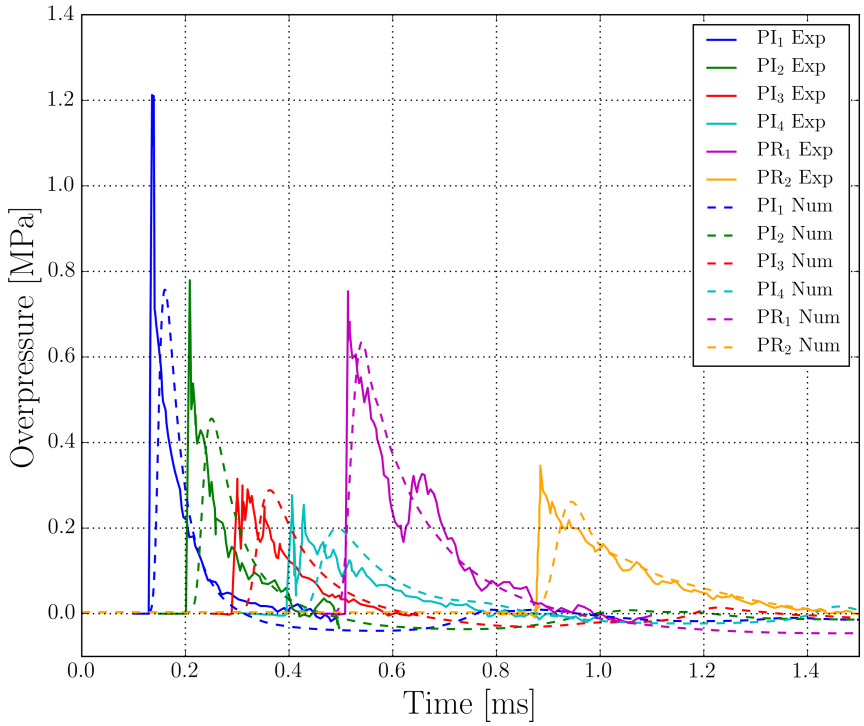

Figure 4: Experimental (solid lines) and numerical (dashed lines) pressure-time histories recorded from the detonation of a 14.2 g hemispherical mass of Formex F4HV [5, 6].

As expected, the blast wave arrives earlier to the transducers closer to the explosive and the peak pressure reduces and the duration of the pulse increases with the distance. These effects are related to the decrease of the magnitude of the overpressure due to the expansion of the wave and decrease of the blast wave velocity with increasing distance from the source [28]. The numerical results regarding incident pressure slightly underestimate pressure peaks and slightly overestimate the time of arrival. The differences in the magnitude of the overpressure are higher in the sensors located closer to the detonation point. This has to do with with the fact that in this area the mesh is coarser than required to reproduce the singularity nature (sharpness) of the signal. Regarding the trend of reduction in the magnitude of the overpressure peak and an increase of the duration of the pressure pulse, for increasing distances to the explosive, the numerical simulations predict similar values of the experimental obtained.

The generated blast wave takes longer to reach pressure transducer PR_1 than PI_4 because the distance to the high-explosive is larger (570 > 500 mm, see Figure 1). However, the overpressure peak is significantly higher in PR_1 than in PI_4. Although the HE is attached to the surface of the incident wall, the detonation generate a 3D blast wave (P_i),

which is free to expand around the air until the surface of the reflected wall. This boundary condition produced a reflected pressure wave (P_r) which interact with the blast wave produced by the explosion, adding an overpressure which is measured by the PR_1 and increasing the pulse duration. Both phenomena measured by the pressure transducer are also predicted by the numerical simulations.

The PR_2 pressure sensor shows a reduction in the recorded overpressure because the magnitude of the incident wave that arrives at this location is lower. Additionally, only part of the blast wave is reflected, as established by the equation proposed by Randers-Peherson et al. [9] in which pressure P is obtained as a function of the incident pressure P_i, reflected pressure P_r and angle of incidence of the wave θ, that is,

$$P = P_i\left(1 + \cos\theta - 2\cos^2\theta\right) + P_r\cos^2\theta \tag{3}$$

From these results it can be said that the proposed numerical model reproduces the increase of overpressure of the reflected wave with a good level of accuracy. However, the numerical model underestimates the overpressure peaks and overestimates the time of arrival.

To improve the consistency of the validation procedure, additional comparisons are made with results from the detonation of a 15 g flat mass of Formex F4HV (see Figure 2(e) [5]). In this case, the difference in the registered overpressure peak is substantial and consequently the results are shown in separate graphs in Figure 5(a) and 5(b). The main consequence of the change in the shape of the explosive is visible in Figure 5(a), where the pressure transducer PR_1 records a peak overpressure over 10 times higher than from the hemispherical explosive with a similar mass. The blast wave also has a shorter time of arrival (0.25 ms compared to 0.50 ms for the hemispherical HE). This effect shows that in this case the blast wave is traveling along the direction perpendicular to the wall at higher speed and with higher magnitude.

The proposed numerical model shows an increase in the magnitude and velocity of the blast wave in sensor PR_1 when compared to the hemispherical HE, albeit still underestimating the peak overpressure, due to the reason explained above. From the results shown in Figure 5 it can also be observed that the blast waves take longer to reach the sensors and their magnitudes are lower than those observed for the hemispherical HE. These effects are well captured by the proposed numerical model.

Similarly to the hemispherical case, the increase of the duration of the pressure pulse with distance is also observed and captured by the numerical model. Due to the combined contribution of the incident and reflected blast waves, pressure sensor PR_2 records a similar overpressure when compared to the hemispherical HE. Thus, the pressure

increase effect in the reflected wave is counterbalanced by the pressure decrease of the incident wave.

The impulse I obtained from the experimental results [5] can be compared to the numerical results. To this end, both scaled impulses ($I/m^{1/3}$, where m is the mass of HE) are shown in Figure 6 for both explosive shapes as a function of the scaled distance ($d/m^{1/3}$) [28]. It can be seen that the proposed numerical model accurately reproduces the impulse registered in each pressure sensor. Table 3 lists the values of each scaled relative impulse in all transducers for both explosive shapes. In most cases the numerical simulations faithfully reproduce the impulse generated by the explosive with average errors around 10%. The error increase with the distance from the detonation point is related to the mesh size. The results in Table 3 include the results of the numerical simulations by Lefrancois et al. [5], where the authors use a two-dimensional (2D) axisymmetrical approach for the problem, adapting the flat shape to an equivalent cylindrical volume. Although this approach does not take into account the three-dimensional (3D) phenomena of the problem studied, the results for the incident wall are accurate. The main issue of the results proposed by Lefrancois et al. [5] has to do with the trend to increase the impulse in the incident wall with the distance, for the flat high-explosive. Note that the 2D axisymmetrical model predicts a decrease for increasing distances, as can be observed in Figure 6.

Concerning the pressures sensors on the incident wall, it can be seen that impulses from the detonation of the hemispherical HE are higher when compared to the flat HE; The hemispherical HE produces a radial homogeneous pressure front. However, the flat HE produces a sharp pressure front focused in the perpendicular direction of the walls. As both explosives have the same mass (and thus the same amount of chemical energy) this higher front in the normal direction leads to a lower pressure wave parallel to the incident wall in the case of the flat explosive. It can also be observed that the impulse from the hemispherical HE decreases with the distance, whilst in the flat case the impulse slightly increase. This is explained by the combination of two effects: (i) the decrease of magnitude of the blast wave with the distance from the source, which lowers the impulse and (ii) the increase of the duration of the pressure pulse due to the blast wave slowdown, which increases the impulse. The combination of these two effects determines the evolution of the impulse with distance. The relative variations of the pressure magnitude (ΔPI [%]) and pressure pulse duration (Δt [%]) at PI_1 and PI_4 are listed in Table 4. For the hemispherical HE the increase of pulse duration does not fully counterbalance the decrease in pressure magnitude and therefore impulse decreases. This effect corroborates the observation that the impulse of the HE is spreading as the pressure wave travels. The lower reduction in pressure magnitude and higher in the duration of the pressure pulse for the flat HE explains the different and converging behaviour of the impulse with distance for the flat HE (Figure 6). The pressure sensors located further away (e.g. PI_4 and PR_2) record similar impulses for the different shape. However, in the near field the pressure sensors (e.g. PI_1 and PI_2) measure noticeable differences. Consequently, the differences in impulse for different HE shapes decreases with the distance [29]; as is expected in the far field the blast wave tends to become hemispherical

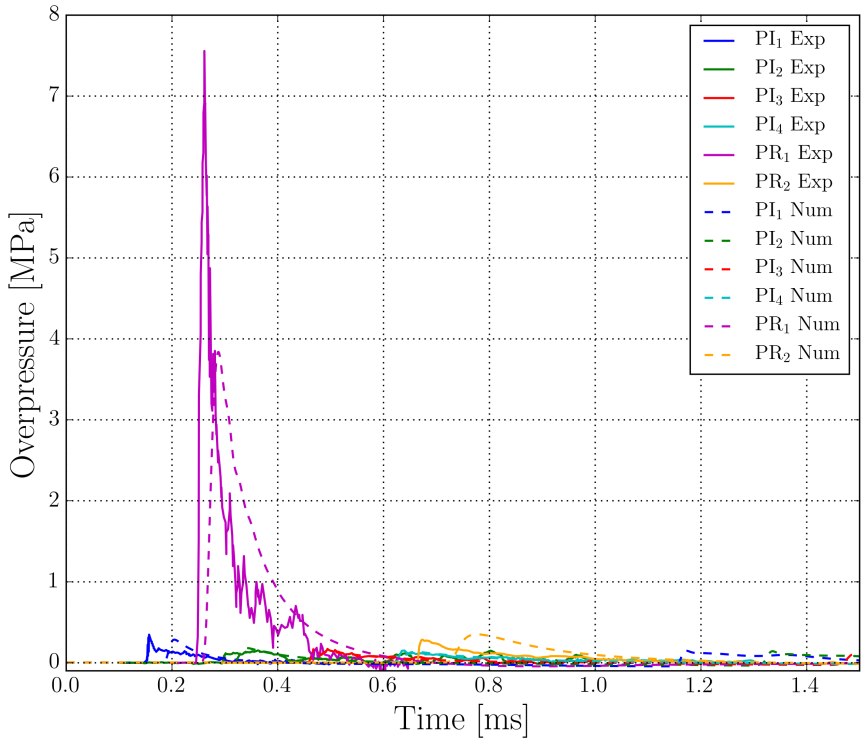

(a)

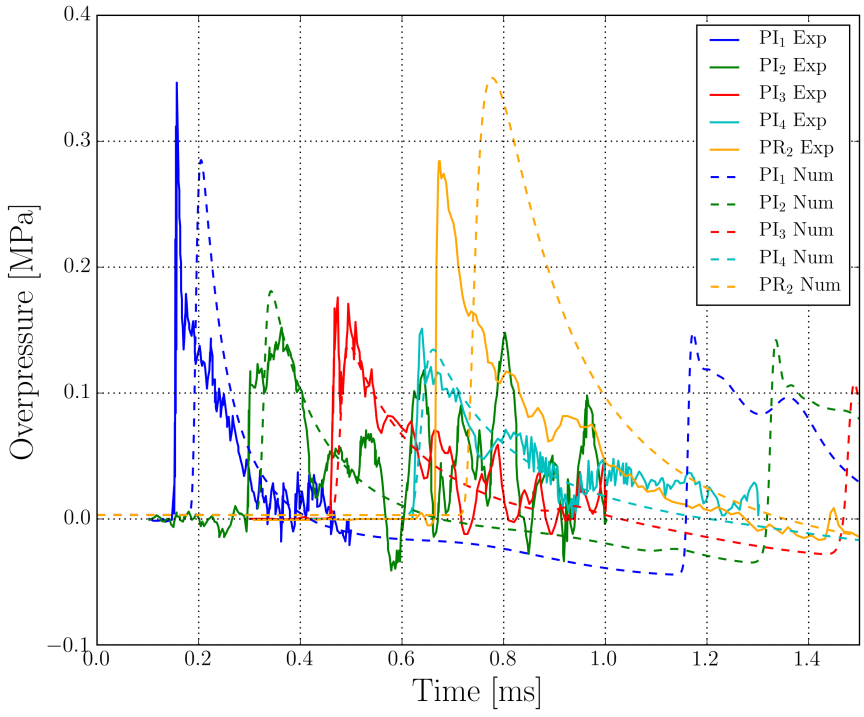

(b)

Figure 5: Experimental and numerical pressure-time histories recorded from the detonation of a 15 g flat mass of Formex F4HV (see Figure 2(e)). Results from (a) all and (b) all but PR_1 pressure transducers [5, 6].

and the influence of the shape of the HE becomes less important. The differences observed regarding the influence of the shape makes the need of a shape analysis more evident. This is discussed in the following section.

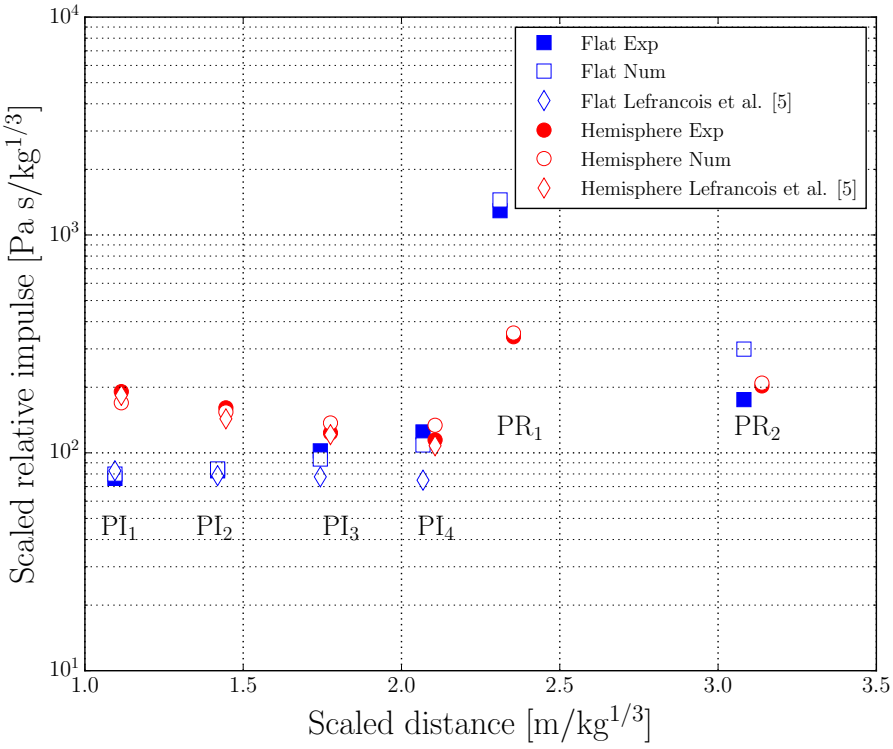

Figure 6: Impulse from all pressure sensors obtained from the numerical model and experimental tests [5, 6].

Although the blast wave was not capture by the high speed video cameras, due to the relation between the deflagration and the blast shape; the images recorded of deflagration are compared to the pressure contours obtained in the numerical simulations at 100 μs in Figure 7. There is a clear similarity between the shapes of both waves. Moreover, the experimental images are in accordance with the pressure values measured in the different transducers, it is seen that the wave velocity from the flat HE is higher perpendicular to the walls than the hemisphere, whilst is the opposite effect in the other direction, same conclusions obtained from the blast wave numerical analysis. The differences between the blast wave generated in the hemispherical case and flat case are also clearly seen in the 3-D numerical images, Figures 7(e) and (f).

The pressure contours at the moment when the reflected wave is initiated for both hemispherical and flat HE are shown in Figure 8. As the blast wave propagates faster along the perpendicular direction to the walls, the reflected wave is generated earlier for the flat HE (at $t \approx 360\ \mu$s, see Figure 8(b)) when compared to the hemispherical HE (at $t \approx 600\ \mu$s, see Figure 8(a)). The magnitude of the pressure peak of the reflected wave is higher for the flat HE, as was

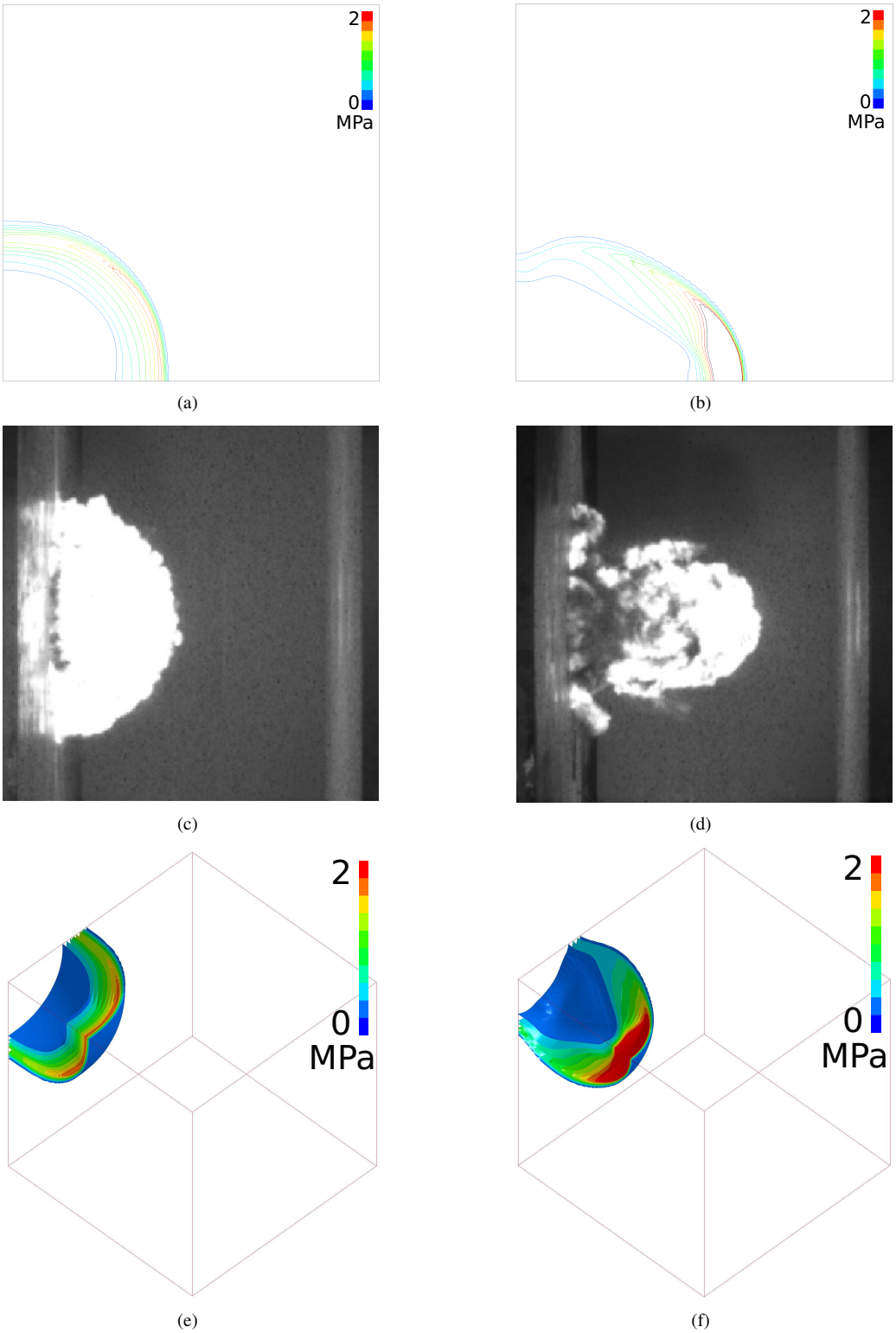

Figure 7: Comparison between numerically obtained pressure contours and deflagration images (by Mespoulet et al. [6]) at 100 μs: (a) numerical and hemispherical HE, (b) numerical and flat HE, (c) experimental and hemispherical HE and (d) experimental and flat HE. 3-D images of pressure contours (e) numerical and hemispherical HE, (f) numerical and flat HE.

Table 3: Scaled relative impulses [Pa s/kg$^{1/3}$] for 14.2 g hemispherical and 15 g flat high-explosives.

		PI_1	PI_2	PI_3	PI_4	PR_1	PR_2
Hemispherical explosive	Experimental	190.98	160.86	123.29	114.61	341.10	202.85
	Numerical	169.72	154.02	137.11	133.77	354.51	208.98
	Error (%)	11.13	4.25	11.21	16.72	3.93	3.02
	Lefrancois et al. [5]	183.4	143.22	121.23	107.76	NA	NA
	Error (%)	3.96	10.96	2.43	5.85	NA	NA
Flat explosive	Experimental	76.30	82.66	102.11	124.71	1292.46	175.54
	Numerical	79.93	84.34	93.66	108.66	1447.58	299.05
	Error (%)	4.76	2.03	8.28	12.87	12.00	70.36
	Lefrancois et al. [5]	82.75	78.59	77.6	74.89	NA	NA
	Error (%)	8.46	4.92	23.99	39.94	NA	NA

Table 4: Pressure magnitudes and pressure pulse durations for the flat and hemispherical high-explosives.

HE Shape	PI_1 [MPa]	PI_4 [MPa]	ΔPI [%]	t_{PI_1} [ms]	t_{PI_4} [ms]	Δt [%]
Hemispherical	1.21	0.274	−77.4	0.27	0.38	+43.3
Flat	0.346	0.151	−56.4	0.23	0.64	+78.3

already recorded by the pressure sensors (Figure 4 and 5). The reflected wave propagates to the air in the opposite direction than the blast wave and can impact again into the incident wall. To better see this phenomenon, the numerical value of the pressure in PI_1, PI_2 and PI_3, and the corresponding relative impulses, are shown in Figure 9. Considering the signal of a single sensor, it can be seen that the first pulse, corresponding to the incident pressure, is in all cases higher for the hemispherical HE. However, for the three sensors, the reflected waves arrive earlier and with higher magnitude for the flat HE. Moreover, in this case the impulse from the reflected wave is higher than the impulse from the incident wave. As such, the effect of the propagation of the reflected wave should not be neglected, most evidently for flat shaped explosives. If the comparison is made considering the differences it the three sensors, an important reduction in the pressure peaks for the incident pressure can be observed, as shown in Figures 4 and 5, while for the reflected wave the pressure magnitude slightly decrease (flat HE) or remains constant (hemispherical HE). This can be explained due to the differences in the distance travelled by the reflected wave before reaching each sensor, which is significantly shorter than in the case of the incident pressure wave. Concerning the impulse, the effect previously observed in Figure 6 is also evident in the incident wave, where a decrease is observed for the hemispherical HE and an increase for the flat HE. However, this behaviour is not visible in the reflected wave due to the wave propagation along the gap between the two walls, as previously discussed.

The proposed numerical model can be used to replicate the generation and dynamics of blast waves with a good level of accuracy, as can be seen from the experimental observations and numerical results presented and discussed above. Nevertheless, it should be noted that discrepancies in the magnitude of the pressure become evident when the pressure pulses cannot be computationally reproduced due to the singularity nature (sharpness) of the signal.

This model will now be used to perform a deeper analysis of the influence of the shape of the high-explosive in the generated blast wave.

A set of numerical simulations are done, using the model described and validated above, to study the influence of the mass and shape of the explosive on the generated blast wave. The corresponding results are presented and discussed below.

3.2. Influence of the mass

The mass of explosive has been proved to be the driving parameter in the generated impulse [28, 30]. In order to further study its effect, 5 different masses were tested, from 10 to 20 g (2 above and 2 below the reference cases) for the flat and hemispherical HE. The mass was varied by increasing the radius in the case of the hemispherical HE and increasing the length and width on the flat HE, keeping the aspect ratio constant.

The results in Figure 10 show the incident and reflected relative impulses and pressure magnitude for the hemispherical and flat HE as a function of the mass of explosive. These impulses were measured in sensors PI_4 and PR_1 at 500 and 570 mm from the location of the explosive (see Figure 1 (a)), respectively. Concerning to the impulse, as expected, increasing the mass of explosive leads to an increase. Although PI_4 is closer to the detonation point than PR_1, the incident impulses are consistently lower due to the constructive interference in the reflected wall. The incident impulse from the flat HE is always lower than the impulse from the hemispherical HE. This trend is, however, inverted in the case of the reflected impulse. The increase in impulse from the hemispherical HE is steeper than from the flat HE as the mass increases. This trend is again inverted for the reflected impulse, which can be explained because explosives with the same mass have the same amount of chemical energy and, therefore, the resulting global impulse in both the incident and reflected walls must be the same. Concerning the pressure magnitudes in PI_4 and PR_1 (Figure 1(b)) it can be seen than same trends and conclusions obtained for the analysis of the impulse can be derived for the pressure data.

3.3. Influence of the shape

From the analysis of how the impulse depends on the initial shape of the HE, observed both experimentally and numerically, it becomes clear that geometry has a major influence. To quantify this, numerical simulations are done with cylindrical HE with different aspect ratios, as defined previously. Cylinders with three different aspect ratios are considered, bounded by the aspect ratio of the hemispherical and the flat high-explosives, as these were previously validated with the experimental tests (see Table 1).

The impulse on the incident wall as a function of the scaled distance is shown in Figure 11 for all the HE shapes. It can be seen that as the aspect ratio increases, the scaled relative impulse also increases. Nevertheless, none of the

cylindrical HE lead to an increase of the impulse with the distance (positive slope). This effect is only visible for the flat HE, which can be explained due to the corner in the other direction. As was explained previously for Figure 6, this effect occurs because the increase produced in the duration of the pressure pulse is higher than the decrease in the magnitude of the pressure. For lower scaled distances (< 1.1) the cylindrical and hemispherical HE with similar aspect ratios deliver the same impulse. This is most probably due to the abrupt change in the geometry at the edges of the cylinder. As the scaled distance increase (> 1.1) this influence becomes less evident.

The impulse on the reflected wall has a different behaviour. When the blast wave hits the wall perpendicularly, the relative impulse decreases with the decrease of the aspect ratio, as can be seen in Figure 12. It can be observed also in Figure 12 that as the distance in the reflected wall increases and, consequently to the point in which the wave impact normally, the magnitude of the reflected impulse decreases. This is explained because the angle of incidence increases and only part of the wave is reflected. This effect leads to a converging trend in the reflected impulse for increasing scaled distances because as Randers-Peherson et al. [9] suggested for spherical charges (see equation 3) the influence of the incident wave increases and the influence of the reflected wave decreases.

A more detailed analysis can be done by looking further into the shape of the pressure waves. The pressure contours for all HE shapes at the same time ($t = 120\ \mu$s) in a 2-D and 3-D views are shown in Figure 13. The detonation of the hemispherical HE generates an almost perfect spherical blast wave, with an almost constant pressure magnitude on the wave front (see Figure 13(a)), leading to a similar magnitude of incident pressure in the incident and reflected directions. The shape of the wave front flattens with the increase of the aspect ratio, with much stronger pressure gradients in the wave front, reaching a maximum along the direction perpendicular to the incident wall. Therefore, a higher impulse is expected on the reflected wall, as is a lower impulse on the incident wall. The maximum aspect ratio, corresponding to the flat HE, leads to a sharp blast wave with the consequent increase on the impulse differences, as shown in Figure 13(e). Additionally, the sharpening of the wave for increasing aspect ratios, increases the incidence angle of the wave compared to the hemispherical HE, which leads to a sharper decrease in the impulse and thus to a crossed tendencies (see Figure 12).

From these observations it can be concluded that the physical problem may be driven by geometrical parameters. The impulse is related to the area perpendicular to the propagation of the blast wave. In order to analyse the effect of the incident and reflected wave, the two corresponding area are obtained, detailed in Figure 14 in grey (reflected wave) and in green (incident wave). The results in this figure show the incident and reflected impulses (PI_4 and PR_1) for all HE shapes as a function of the two frontal areas. There is a clear trend on the impulse, with a stronger variation on the reflected impulses. Therefore, it can be concluded that the changes of the shape of the blast wave, the magnitude of the pressure and the wave velocity are driven by the area of the HE perpendicular to the propagation of the blast

wave, for a constant mass of HE.

4. Conclusions

A numerical model to analyse the influence of the shape of the explosive shape on the generated pressure wave was developed in this work. The model was validated by comparing the numerical results with experimental data obtained from Lefrancois et al. [5] and Mespoulet et al. [6], based on the detonation of hemispherical and flat-shaped high-explosives. The proposed numerical model was used to analyse the influence of the mass and shape of the HE on the pressure profiles, blast wave front geometry and resulting impulses. From the analysis and discussion of results the following main conclusions were drawn:

- The MM-ALE technique implemented in the commercial FEM code LS-DYNA v. R7 is suitable to reproduce the blast wave configuration and pressure magnitude for hemispherical and flat high-explosives. Alternative approaches such as CONWEP or the Lagrangian method are not reliable.

- As expected, the magnitudes of the pressure pulse and impulse registered on reflected walls are significantly higher than on incident walls, due to the interaction of reflected and incident pressure waves. Therefore, the structural and dynamic effects of the reflected pressure pulses should always be taken into account. This becomes more relevant when analysing closed structures where the number of reflections can be significant.

- The magnitude of the pressure pulse and wave velocity resulting from the detonation of a hemispherical HE is consistently equal along all radial directions. For flat explosives, however, the magnitude of the pressure pulse and velocity is significantly higher along the direction perpendicular to the wall. Therefore, the most severe scenario corresponds to a structure at right angles to the flat explosive. Nevertheless, from an energetic point of view, as the same mass of explosive will have the same chemical energy, the resulting global impulse is constant.

- The numerical model developed, validated and tested by the authors can be reliably used to study the influence of the aspect ratio of the high-explosive on the generated pressure waves and the impulses. To this end, explosive cylinders varying from the aspect ratio of the hemispherical to the flat shape were studied, leading to the global conclusion that the driver parameter in the impulse is the initial area of the high-explosive perpendicular to the propagation of the blast wave.

Acknowledgements

This research was done with the financial support of the mobility internship for researchers of Carlos III University of Madrid (Spain) ("Programa propio de investigación - Convocatoria 2014 movilidad").

References

[1] A. M. Benselama, M. J.-P. William-Louis, F. Monnoyer, C. Proust, A numerical study of the evolution of the blast wave shape in tunnels, Journal of Hazardous Materials 181 (13) (2010) 609 – 616.

[2] M. Larcher, F. Casadei, G. Solomos, Influence of venting areas on the air blast pressure inside tubular structures like railway carriages, Journal of Hazardous Materials 183 (13) (2010) 839 – 846.

[3] J. Clutter, M. Stahl, Hydrocode simulations of air and water shocks for facility vulnerability assessments, Journal of Hazardous Materials 106 (1) (2004) 9 – 24.

[4] B. Vanderstraeten, M. Lefebvre, J. Berghmans, Heat and mass transfer in chemical process industry accidents a simple blast wave model for bursting spheres based on numerical simulation, Journal of Hazardous Materials 46 (2) (1996) 145 – 157.

[5] A. Lefrancois, S. Chapelle, S. Pauly, J. Mespoulet, Tremendous increase of the blast effect above HE plates characterised by small scale experiments, MABS 20 Oslo (Norway) (September 2008).

[6] J. Mespoulet, F. Plassard, P. Hereil, A. Lefrancois, Influence of HE shape on blast profile, Eight European LS-DYNA users conference similation. Strasbourg (Germany) (May 2011).

[7] Livermore Software Technology Company, Keyword User's Manual, LS-DYNA R8.0 (March 2015).

[8] U.S. Army Engineer Waterboys Experiment Station, Collection of conventional weapon effects calculations based on TM 5-855-1, Fundamentals of Protective Design for Conventional Weapons (1992).

[9] G. Randers-Pehrson, K. Bannister, Airblast loading model for DYNA2D and DYNA3D, US Army Resarch Laboratory ARL-TR-1310 (March 1997).

[10] B. Ostraich, O. Sadot, O. Levintant, I. Anteby, G. Ben-Dor, A method for transforming a full computation of the effects of a complex-explosion scenario to a simple computation by conwep, Shock Waves 21 (2) (2011) 101–109.

[11] D. Jenson, V. Unnikrishnan, Energy dissipation of nanocomposite based helmets for blast-induced traumatic brain injury mitigation, Compos. Struct. 121 (2015) 211 – 216.

[12] Z. Tabatabaei, J. Volz, J. Baird, B. Gliha, D. Keener, Experimental and numerical analyses of long carbon fiber reinforced concrete panels exposed to blast loading, Int. J. Impact Eng. 57 (2013) 70 – 80.

[13] U. Nystrm, K. Gylltoft, Numerical studies of the combined effects of blast and fragment loading, Int. J. Impact Eng. 36 (8) (2009) 995 – 1005.

[14] A. Neuberger, S. Peles, D. Rittel, Scaling the response of circular plates subjected to large and close-range spherical explosions. Part I: Air-blast loading, Int. J. Impact Eng. 34 (5) (2007) 859 – 873.

[15] A. Neuberger, S. Peles, D. Rittel, Scaling the response of circular plates subjected to large and close-range spherical explosions. Part II: Buried charges, Int. J. Impact Eng. 34 (5) (2007) 874 – 882.

[16] B. Zakrisson, B. Wikman, H. Hggblad, Numerical simulations of blast loads and structural deformation from near-field explosions in air, Int. J. Impact Eng. 38 (7) (2011) 597 – 612.

[17] M. Anghileri, L. Castelletti, M. Tirelli, Fluid-structure interaction of water filled tanks during the impact with the ground, Int. J. Impact Eng. 31 (3) (2005) 235 – 254.

[18] J. Pernas-Sánchez, D. Pedroche, D. Varas, J. López-Puente, R. Zaera, Numerical modeling of ice behavior under high velocity impacts, Int. J. Solids Struct. 49 (14) (2012) 1919 – 1927.

[19] J. Donea, A. Huerta, J. P. Ponthot, A. Rodríguez-Ferran, Arbitrary Lagrangian-Eulerian Methods, in: E. Stein, R. D. Borst, T. J. R. Hughes (Eds.), Encyclopedia of Computational Mechanics, Wiley, 2004, Ch. 14, pp. 413–433.

[20] K. Hughes, R. Vignjevic, J. Campbell, T. D. Vuyst, N. Djordjevic, L. Papagiannis, From aerospace to offshore: Bridging the numerical simulation gaps-simulation advancements for fluid structure interaction problems, Int. J. Impact Eng. 61 (2013) 48 – 63.

[21] D. Varas, R. Zaera, J. López-Puente, Numerical modelling of the hydrodynamic ram phenomenon, Int. J. Impact Eng. 36 (3) (2009) 363 – 374.

[22] D. Varas, R. Zaera, J. López-Puente, Numerical modelling of partially filled aircraft fuel tanks submitted to Hydrodynamic Ram, Aerosp. Sci. Technol. 16 (1) (2012) 19 – 28.

[23] J. Artero-Guerrero, J. Pernas-Sánchez, D. Varas, J. López-Puente, Numerical analysis of CFRP fluid-filled tubes subjected to high-velocity impact, Compos. Struct. 96 (2013) 286 – 297.

[24] J. Artero-Guerrero, J. Pernas-Sánchez, J. López-Puente, D. Varas, On the influence of filling level in CFRP aircraft fuel tank subjected to high velocity impacts, Compos. Struct. 107 (2014) 570 – 577.

[25] B. Dobratz, P. Crawford, Llnl explosives handbook: Properties of chemical explosives and explosive simulants, Report UCRL-5299; Rev.2 (1985).

[26] EURENCO-Groupe SNPE, Formex, Datasheet (2013).

[27] Z. Tabatabaei, J. Volz, A comparison between three different blast methods in LS-DYNA: LBE, MM-ALE, coupling of LBE and MM-ALE, 12th International LS-DYNA Users Conference (2012).

[28] US Army, Structures to resist the effects of accidental explosions, Technical Manual TM5-1300 (November 1990).

[29] US Army, Capabilities of atomic weapons, Technical Manual TM 23-200 (November 1957).

[30] N. Huffington, W. Ewing, Reflected impulse near spherical charges, Technical report BRL-TR-2678 AD-A160 797 (September 1985).

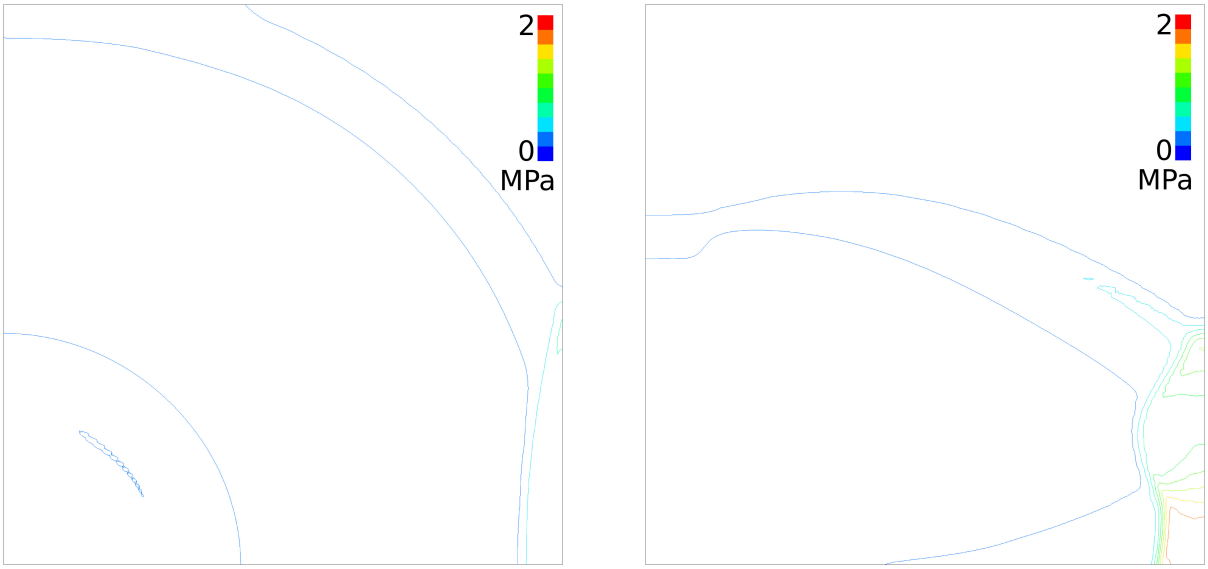

(a) (b)

Figure 8: Numerically obtained pressure contours at the moment the reflected wave becomes visible in the numerical simulations for the following initial high-explosive shapes: (a) hemispherical @ $t = 600\,\mu$s and (b) flat @ $t = 360\,\mu$s.

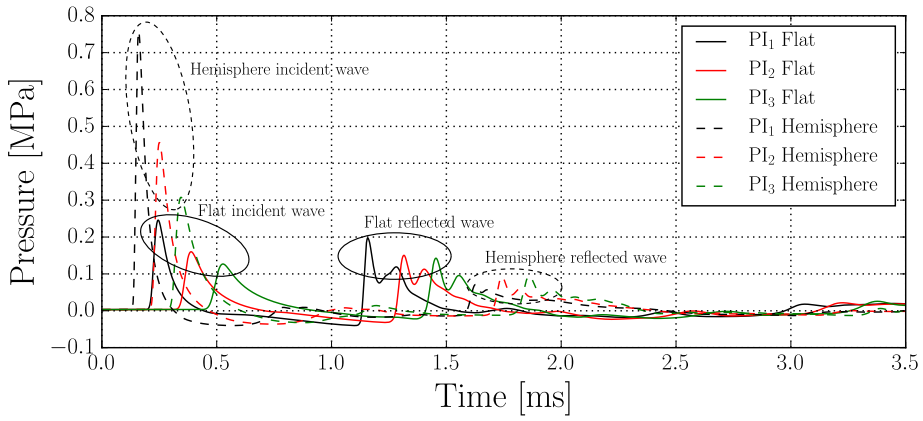

(a)

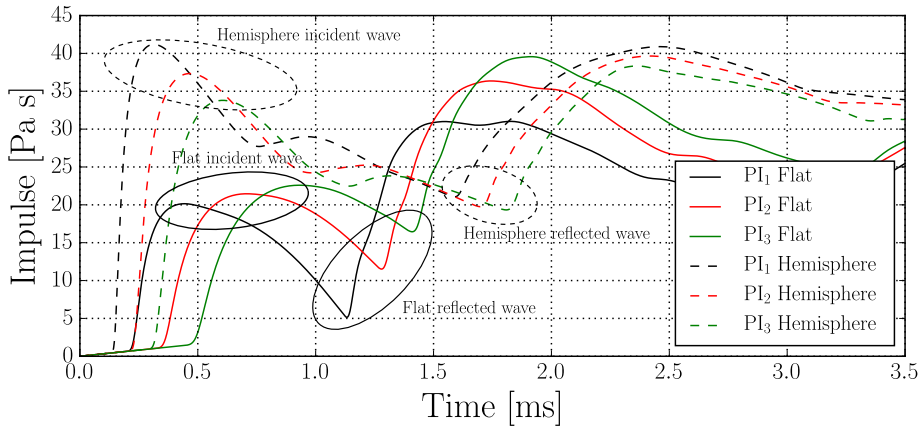

(b)

Figure 9: (a) Pressure-time history and (b) impulse-time history as recorded in pressure sensors PI_1, PI_2 and PI_3.

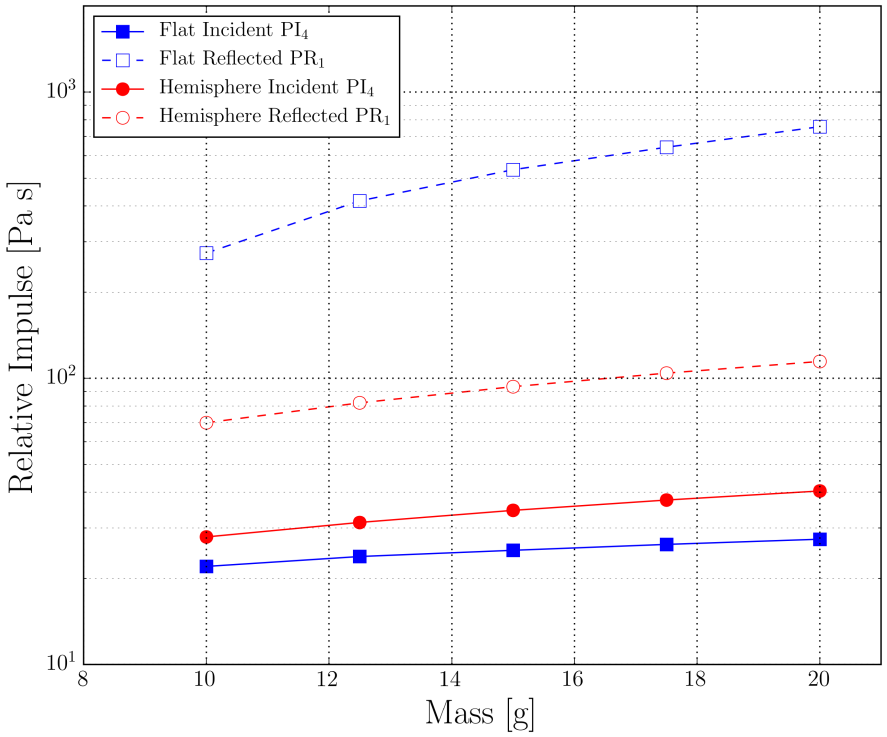

(a)

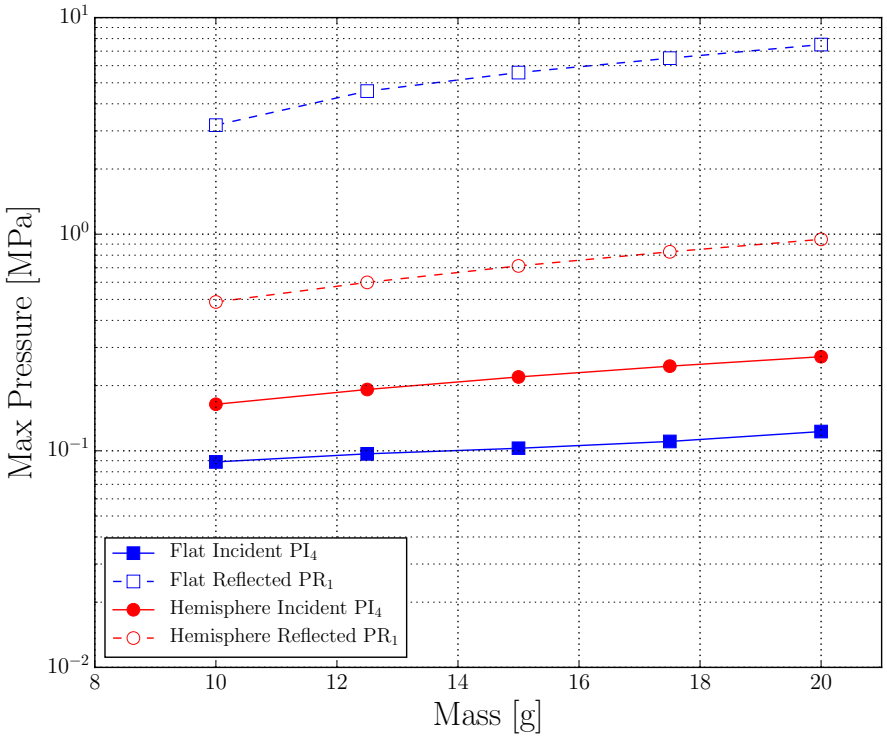

(b)

Figure 10: (a) Incident and reflected impulse and (b) pressure dependency of the in PI_4 and PR_1 on the mass of explosive.

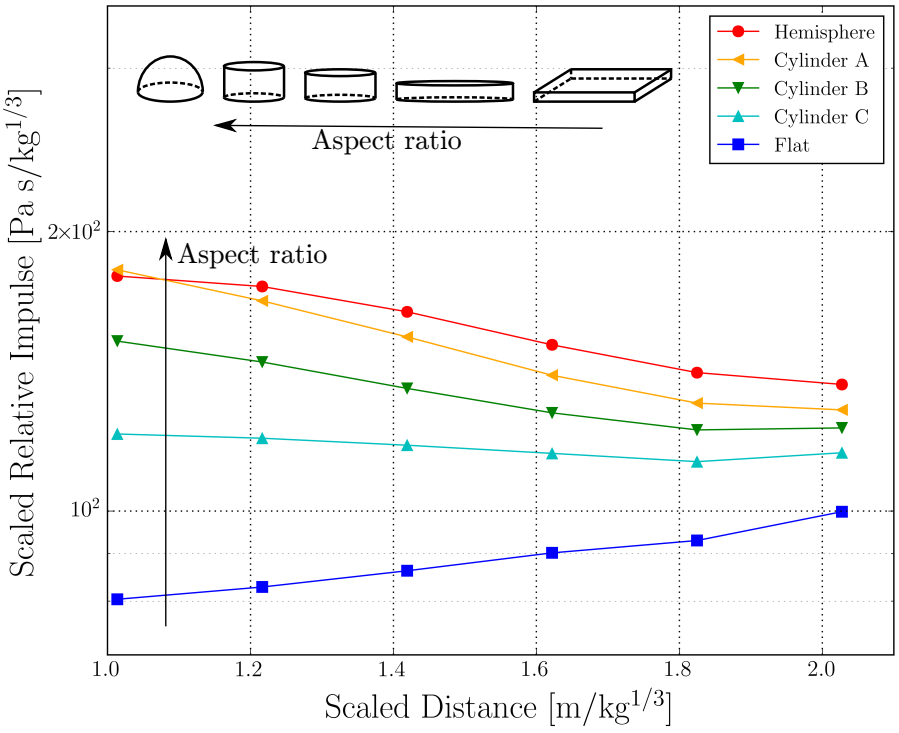

Figure 11: Impulse on the incident wall for all shapes and aspect ratios.

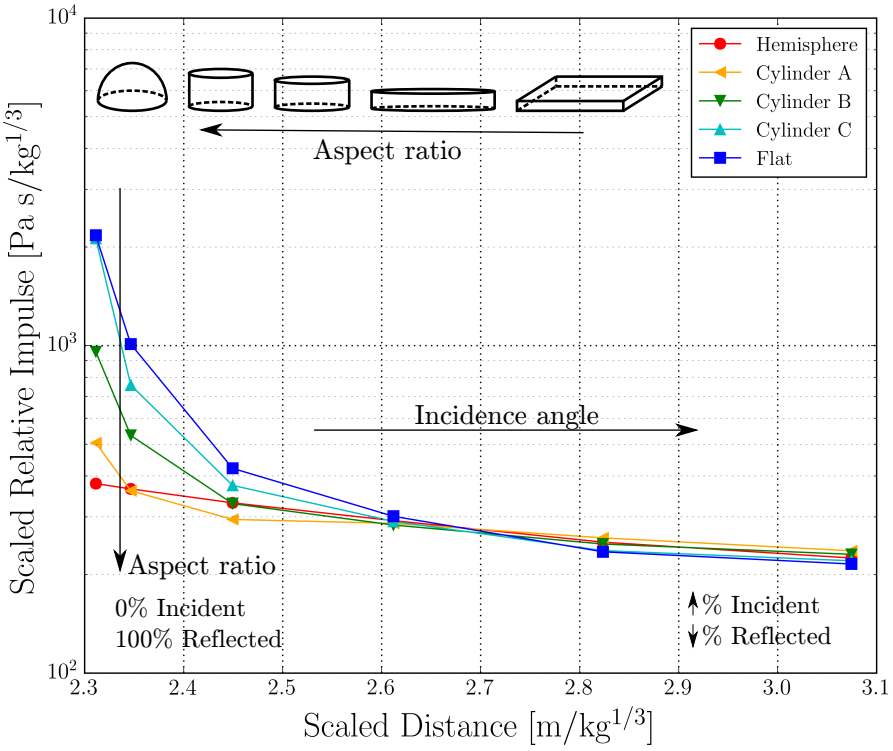

Figure 12: Impulse on the reflected wall for all shapes and aspect ratios.

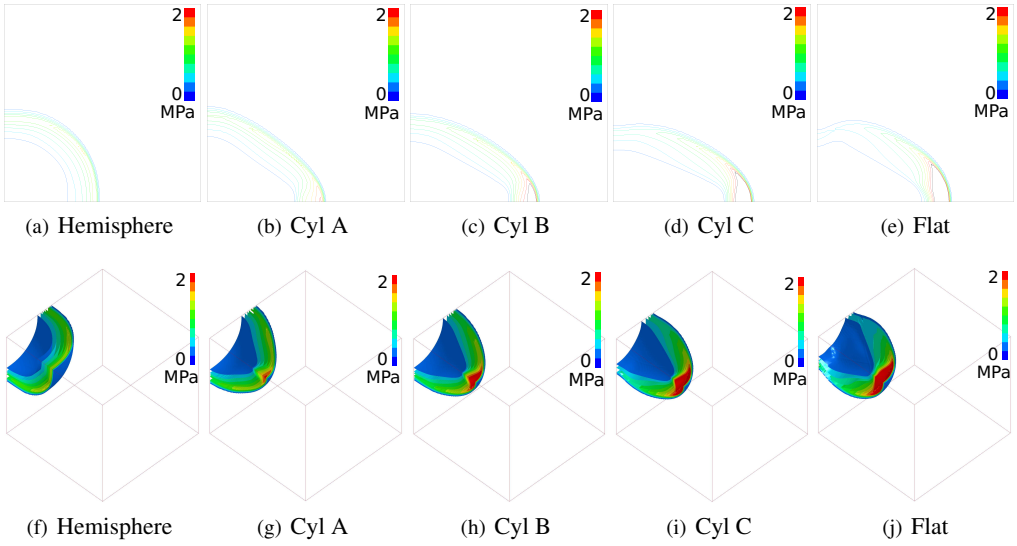

Figure 13: (a)-(e) 2-D Pressure contour and (f)-(j) 3-D pressure contour for the different shapes at $t = 120\,\mu s$.

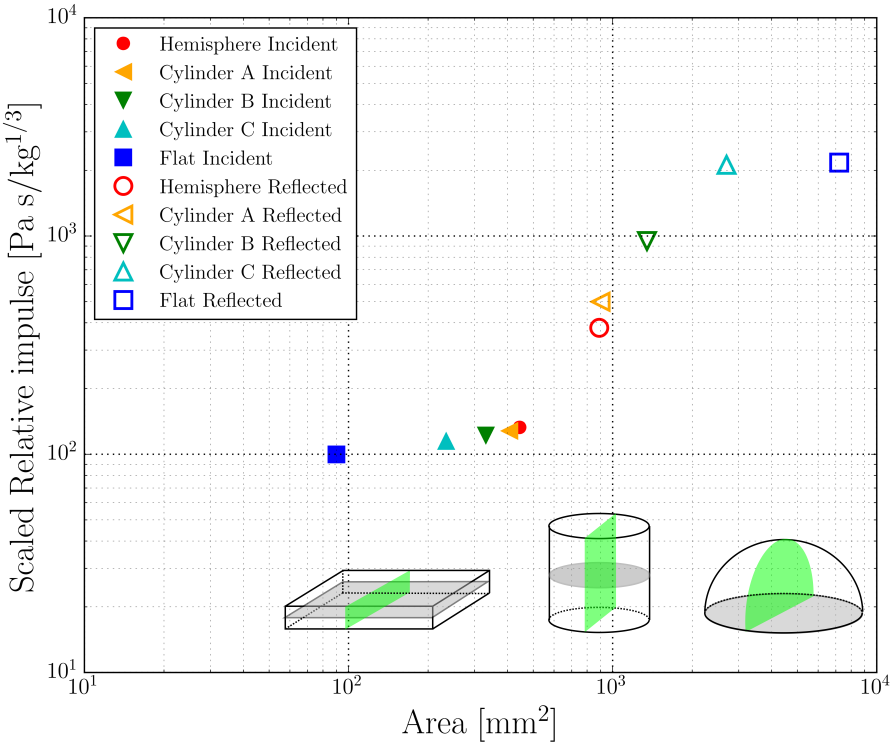

Figure 14: Relative impulse versus the area of the high-explosive perpendicular to the propagation of the blast wave.